

XIE, Y., WANG, S., FERNANDEZ, C., YU, C., FAN, Y., CAO, W. and CHEN, X. 2021. Improved gray wolf particle filtering and high-fidelity second-order autoregressive equivalent modeling for intelligent state of charge prediction of lithium-ion batteries. *International journal of energy research* [online], 45(13), pages 19203-19214. Available from: <https://doi.org/10.1002/er.7014>

Improved gray wolf particle filtering and high-fidelity second-order autoregressive equivalent modeling for intelligent state of charge prediction of lithium-ion batteries.

XIE, Y., WANG, S., FERNANDEZ, C., YU, C., FAN, Y., CAO, W. and CHEN, X.

2021

This is the peer reviewed version of the following article: XIE, Y., WANG, S., FERNANDEZ, C., YU, C., FAN, Y., CAO, W. and CHEN, X. 2021. Improved gray wolf particle filtering and high-fidelity second-order autoregressive equivalent modeling for intelligent state of charge prediction of lithium-ion batteries. International journal of energy research, 45(13), pages 19203-19214, which has been published in final form at <https://doi.org/10.1002/er.7014>. This article may be used for non-commercial purposes in accordance with [Wiley Terms and Conditions for Use of Self-Archived Versions](#).

**Improved Gray Wolf Particle Filtering and High-fidelity
 Second-order Autoregressive Equivalent Modeling for
 Intelligent State of Charge Prediction of Lithium-ion
 Batteries**

Journal:	<i>International Journal of Energy Research</i>
Manuscript ID	ER-21-19930.R2
Wiley - Manuscript type:	Research Article
Date Submitted by the Author:	25-May-2021
Complete List of Authors:	Xie, Yanxin Wang, Shunli; Southwest University of Science and Technology, School of Information Engineering Fernandez, Carlos; Robert Gordon University Yu, Chun-Mei; Southwest University of Science and Technology Fan, Yongcun Cao, Wen; Southwest University of Science and Technology, School of Information Engineering Chen, Xianpei
Keywords:	state of charge, lithium-ion batteries, high-fidelity second-order autoregressive model, gray wolf particle filtering

SCHOLARONE™
 Manuscripts

Improved Gray Wolf Particle Filtering and High-fidelity Second-order Autoregressive Equivalent Modeling for Intelligent State of Charge Prediction of Lithium-ion Batteries

Yanxin Xie^a, Shunli Wang^{a*}, Carlos Fernandez^b, Chunmei Yu^a, Yongcun Fan^a, Wen Cao^a, Xianpei Chen^a

^a*School of Information Engineering, Southwest University of Science and Technology, Mianyang 621010, China;*

^b*School of Pharmacy and Life Sciences, Robert Gordon University, Aberdeen AB10-7GJ, UK.*

Abstract: The rapid development of new energy vehicles puts forward higher requirements for the lithium-ion batteries model construction, high-efficiency condition monitoring and collaborative estimation. An improved high-fidelity second-order autoregressive model is proposed and constructed, and the autoregressive model is integrated with the second-order equivalent circuit model, which can achieve an accurate and reliable description of the batteries internal dynamic change process. To achieve the accurate expression of the battery's external characteristics and internal state, the forgetting factor is combined with the recursive least square algorithm to improve the parameter identification accuracy and optimality while reducing the space complexity of the algorithm. A novel gray wolf particle filtering algorithm is proposed, which eliminates the particles severe degradation in traditional algorithms and enhances the ability of particles to resist degradation. The algorithm superiority and generalization are verified under complex working conditions. The experimental results show that the accuracy of the high-fidelity second-order autoregressive model can reach 99%, which can well simulate the complex chemical reaction process inside the lithium-ion battery. Experimental simulation is performed under constant current conditions. Compared with the extended Kalman filter, unscented Kalman filter, and particle filter algorithms, the gray wolf particle filter algorithm has reduced the root mean square error by 3.39%, 0.90%, 2.84%, and the mean absolute error has reduced by 1.95%, 0.51%, 2.22%. Under dynamic stress test conditions, the root mean square error is reduced by 1.54%, 0.33%, and 0.78%, and the average absolute error is reduced by 1.4%, 0.22%, and 0.76%. In addition, when tested under different environmental conditions, although the improved algorithm has a relatively long running time, the estimation accuracy of the algorithm is greatly improved and the execution efficiency is high. The improved algorithm provides a theoretical basis for the reliability and stability of the onboard operation of lithium-ion batteries.

Key words: state of charge; lithium-ion batteries; high-fidelity second-order autoregressive model; gray wolf particle filtering

***Corresponding author:** Shunli Wang. Tel: +86-15884655563. E-mail address: 497420789@qq.com.

1. Introduction

With the structural changes in the global energy supply, battery management systems (BMS) have become the main direction of technological innovation in the new energy industry [1, 2]. The functions of the BMS are gradually improved, and the occurrence of abnormal phenomena such as battery over-charging, over-discharging, and overheating has been effectively prevented with the advancement of science and technology [3]. This greatly increases the battery's cruising range and prolongs its service life, ensuring the battery safe and reliable operation [4, 5]. Lithium-ion batteries (LIBs) are an important part of the BMS. Throughout the life cycle of the battery, the differences between the cells and their significant accumulation, and the unreasonable attenuation of cycle life have become the core elements that restrict the current stage development. The reason for this phenomenon lies in the imperfect understanding of the LIBs working characteristics and operating mechanism, and the failure to form a reliable

model construction and state prediction optimization mechanism. Therefore, to describe the reaction mechanism of LIBs more intuitively, an equivalent circuit model is constructed. This provides accurate and effective input parameters for the subsequent LIBs state estimation [6]. The accurate LIBs state of charge (SOC) estimation can prevent irreversible damage to the batteries due to overcharge and over-discharge, which is of great significance to further accurately predict the batteries' life [7-10].

LIBs have strong nonlinear dynamic characteristics due to the combination of multiple parameters coupling processes. Considering the aging of the LIB itself and the complexity and variability of the environment. To simulate the voltage response characteristics under different load conditions, the existing research divides the equivalent model into three types: black box model, electrochemical mechanism model, and semi-mechanical and semi-empirical model [11-13]. The black box model is mainly used to characterize the voltage response characteristics. It is a non-linear mapping

1 function. The data is used to train the model without
2 considering the internal mechanism and structure, but it is
3 heavily dependent on the experimental data. The
4 electrochemical model (EM) is aimed at the LIBs complex
5 dynamic characteristics and can accurately simulate the
6 electrochemical reaction process inside the battery. Xiong
7 et al. [14] proposed an EM to effectively describe the
8 physical and chemical behavior of batteries. However, there
9 are many identification parameters and the construction
10 structure is complicated. The semi-mechanical and semi-
11 empirical model can describe the electrochemical
12 characteristics through simple circuit components, and use
13 mathematical expressions to simulate the battery dynamic
14 behavior. The equivalent circuit model (ECM) has clear
15 physical meaning and simple mathematical expressions.
16 Therefore, it is widely used in describing the batteries
17 electrochemical characteristics and has good adaptability.
18 Zhang et al. [15] studied and compared the first-order and
19 second-order RC models, and clarified the model selection
20 in the actual control system. He et al. [16] considered the
21 hysteresis characteristics of the open circuit voltage (OCV),
22 explored and proposed a variable parameter equivalent
23 hysteresis model based on Thevenin model. Wu et al. [17]
24 employed that the temperature-compensated Thevenin
25 ECM accurately reflects the batteries dynamic
26 characteristics. Wang et al. [18] presented a splicing-
27 equivalent circuit model (SECM) to achieve LIB packs
28 accurate mathematical expression during complex working
29 conditions. The ECM structure is simple and easy to analyze,
30 which is particularly important for energy management and
31 has become the batteries modeling mainstream direction.

32 In recent years, new energy vehicles have developed
33 rapidly, and SOC estimation algorithms have emerged in an
34 endless stream. The traditional basic SOC estimation
35 methods include OCV method, internal resistance method
36 and Ampere-hour (Ah) method [19-23]. However, these
37 approaches have the following weaknesses. First, the
38 batteries state at the initial moment is not easy to determine
39 and there is a certain error in accuracy. Second, only when
40 the batteries are left standing for a long time, the accuracy
41 of the batteries state estimation is high, but it is not
42 applicable to actual working conditions. Third, ignore
43 batteries aging process the influence of the energy density
44 and cycle life on the estimation. In order to overcome the
45 above-mentioned problems, modern SOC estimation

46 methods developed by modern adaptive control theory have
47 been successively proposed. Among them, the most classic
48 state estimation algorithm is the Kalman filter (KF)
49 algorithm, which makes the best estimation of the state of
50 the dynamic system [24-29]. After multiple iterative
51 updates, the estimation result is close to the true value, the
52 initial value of the capacity is corrected efficiently, and the
53 anti-interference ability is strong. Yang et al. [30] employed
54 extended Kalman filter (EKF) for SOC estimate. It is not
55 necessary to know the SOC value and the OCV value in
56 advance, and the SOC can be estimated in real time.
57 However, EKF is the local linearization result, which
58 greatly increases the estimation error. And it is related to the
59 statistical characteristics of the state noise and the
60 observation noise, which will affect the filter divergence.
61 Therefore, Ben et al. [31] and Zhu et al. [32] employed
62 unscented Kalman filter (UKF) algorithm to estimate the
63 SOC in response to the EKF algorithm problems. Zhang et
64 al. [33] proposed an adaptive unscented Kalman filter
65 (AUKF) algorithm to accurately estimate the SOC online.
66 And it solves the problem that the error covariance matrix
67 is a non-positive definite matrix. Liu et al. [34] utilized the
68 particle filter (PF) algorithm to estimate the SOC. Unlike
69 the KF algorithm, it is not limited by linearization errors and
70 Gaussian noise assumptions, and is suitable for any state
71 and measurement model in any environment [35-37]. In
72 order to improve the LIBs status observation accuracy,
73 Wang et al. [39] proposed an unscented particle filtering
74 (UPF) method and obtained the best remaining discharge
75 prediction time. To prevent particle degradation, Wei et al.
76 [38] adjusted the adaptive factor composed of prediction
77 residuals, thereby avoiding the disturbance of abnormal
78 observation and the kinematic model noise. However, its
79 sensitivity performance is not specifically analyzed.

80 In addition, many other modern SOC estimation methods
81 are also being proposed and studied. The neural network
82 (NN) method is suitable for all kinds of batteries. The
83 battery is regarded as a black box, and the mapping data
84 between input parameters and output parameters is
85 extracted, and then it is determined by repeated trials during
86 training [4, 40-42]. However, it requires a lot of data, and
87 the estimation structure is greatly affected by the training
88 data and methods. Therefore, in practical applications, the
89 hardware requirements are extremely high due to the
90 complexity of the algorithm. Support vector machine (SVM)

algorithm is also a data-driven approach, which has good adaptability to nonlinear problems [41, 43, 44]. However, similar to the neural network method, the dependence on training data and the complexity of the algorithm are both high.

The method used in this paper for original contributions differs from that used in the preceding literature. First, to improve the fidelity of the battery equivalent model, a high-fidelity second-order autoregressive model is proposed and constructed. Secondly, using the iterative recursive method, combined with previous data, considering the forgetting factor influence, obtain the best model parameters. Finally, a novel gray wolf particle filter (GWPF) algorithm is proposed to overcome the problem of particle degradation. To characterize the superiority over the proposed algorithm, it compares and analyzes with the traditional SOC estimation methods, and obtains the experimental data analysis results.

2. Mathematical analysis

2.1. High-fidelity second-order autoregressive model construction

Accurate battery modeling is a prerequisite for the high-precision state of charge evaluation. Aiming at the goal of simulating the LIB working process, based on the experimental design to obtain the LIB external characteristic parameters, a battery ECM is constructed. Characterize the complex electrochemical reaction mechanism inside the battery, clarify the corresponding relationship between the battery external characteristics and the internal state, and analyze the experimental data to determine the state parameters.

To accurately and reliably reflect the dynamic change process inside the battery considering the polarization effect, the autoregressive model and the second-order equivalent circuit model are combined. Through online processing of time, predict the time-varying parameters at the next moment. The second-order equivalent circuit model is shown in Fig. 1.

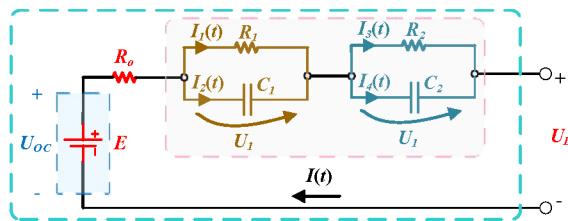


Fig. 1. Second-order equivalent circuit model

In Fig. 1, U_{oc} is the open circuit voltage. R_o is the ohm internal resistance. R_1 and R_2 represent polarization internal resistance and surface effect internal resistance, respectively. C_1 and C_2 represent polarization capacitance and surface effect capacitance respectively. $I(t)$ is the actual current flowing through the load. U_L is the closed-circuit voltage of the external load. By analyzing the model structure, according to Kirchoff's law, the mathematical expression of its circuit dynamic model is obtained in Eq. (1).

$$\begin{cases} U_L = U_{oc} - IR_o - U_1 - U_2 \\ I = U_1/R_1 + C_1 dU_1/dt \\ I = U_2/R_2 + C_2 dU_2/dt \end{cases} \quad (1)$$

According to the obtained battery second-order differential network model, it is substituted into the linear regression equation of the autoregressive model, as shown in Eq. (2).

$$y(k) = \varphi^T(k) \vartheta(k-1) + e(k) \quad (2)$$

Among them, $\varphi^T(k)$ is the system input vector, $\vartheta(k-1)$ is the coefficient vector, and the corresponding vector is shown in Eq. (3). $e(k)$ is the relative error between theory and practice. $y(k)$ is the output of the system.

$$\begin{cases} \vartheta(k) = [a_1; a_2; b_0; b_1; b_2] \\ \varphi(k) = [-y(k-1); -y(k-2); x(k); x(k-1); x(k-2)] \end{cases} \quad (3)$$

From the Laplace transform, the transfer function $G(s)$ of the dynamic system is obtained, as shown in Eq. (4).

$$G(s) = \frac{U_L(s) - U_{oc}(s)}{I(s)} = \frac{c_2 s^2 + c_3 s/c_1 + c_4/c_1}{s^2 + c_3 s/c_1 + 1/c_1} \quad (4)$$

Among them, the expression of parameter c is shown in Tab. 1.

Tab. 1 Custom parameter c expression

Parameter	Expression
c_1	$R_1 C_1 R_2 C_2$
c_2	R_o
c_3	$R_o R_1 C_1 + R_o R_2 C_2 + R_1 R_2 C_2 + R_1 R_2 C_2$
c_4	$R_o + R_1 + R_2$
c_5	$R_1 C_1 + R_2 C_2$

Discretize $G(s)$, and substitute $s = (1-z^{-1})/Tz^{-1}$ into Eq. (4) to obtain the parameter expression of the coefficient vector $\vartheta(k)$, as shown in Tab. 2.

Tab. 2 $\vartheta(k)$ parameter expression

Parameter	Expression
-----------	------------

a_1	$2-c_5T/c_1$
a_2	$c_5T/c_1-T^2/c_1-1$
b_0	c_2
b_1	c_3T/c_1-2c_2
b_2	$c_4T^2/c_1-c_3T/c_1+c_2$

The ECM is rewritten as a discretized time series, and the differential equation in the time domain is obtained.

$$U_L(k) - U_{oc}(k) = -a_1[U_L(k-1) - U_{oc}(k-1)] - a_2[U_L(k-2) - U_{oc}(k-2)] + b_0I(k) + b_1I(k-1) + b_2I(k-2) \quad (5)$$

Among them, k is the time signal of the sampling sequence.

2.2. Online full-parameter identification based forgetting factor recursive least square method

The recursive least square (RLS) method is widely used in numerical optimization problems. It finds the data best function match by minimizing the sum of squared errors, and can give the best parameter fitting results in a statistical sense. Based on the RLS, adding a forgetting factor to reduce the amount of old data in the covariance matrix can effectively prevent data saturation in the RLS algorithm. As an effective method to solve this problem, in order to obtain the coefficient matrix $\mathcal{G}(k)$, the mathematical derivation process is as follows.

Step 1: Forecast estimation error $e(k)$.

$$e(k) = U_L(k) - U_{oc}(k) - \varphi^T(k) - 1 \quad (6)$$

Step 2: Update the gain $K(k)$.

$$K(k) = P(k-1) - \varphi(k)[\lambda \cdot I + \varphi^T(k) \cdot P(k-1)\varphi(k)]^{-1} \quad (7)$$

λ is the forgetting factor, with a value between 0.95 and 0.99.

Step 3: Calculate the error covariance matrix $P(k)$.

$$P(k) = [I - K(k) \cdot \varphi^T(k)] \cdot P(k-1) / \lambda \quad (8)$$

Step 4: Obtain the coefficient matrix $\mathcal{G}(k)$.

$$\mathcal{G}(k) = \mathcal{G}(k-1) + K(k)e(k) \quad (9)$$

Step 5: Repeat **steps 1 ~ 4** until the parameter identification at all times is completed.

Thus, the parameter values of the second-order autoregressive model can be identified. Therefore, the pseudo code for the least squares online parameter identification based on the forgetting factor is shown in Tab. 3.

Tab. 3 Forgetting factor recursive least square method

Algorithm 1. Pseudo-code of model parameter identification

1. **Procedure** Model parameter identification
2. Given the initial value, the forgetting factor is 0.985.
3. **for** $k = 1, \dots, N$ **do**
4. Update the gain coefficient matrix $K(k)$ using Eq. (7)
5. Calculate the error $e(k)$ between the voltage actual value and theoretical value using Eq. (6)
6. Calculate the error covariance matrix $P(k)$ using Eq. (8)
7. Calculate parameter vector $\mathcal{G}(k)$ using Eq. (9)
8. Calculate model parameters
9. The newly obtained parameters are used as the old parameters for the next recursion.
10. **end for**
11. **end while**
12. **end procedure**

2.3. Gray wolf particle filtering algorithm

In view of the serious particle degradation phenomenon in the traditional PF algorithm, the gray wolf algorithm is now used for optimization, which effectively increases the particle diversity and enhances the particle's anti-degradation ability. Gray wolf optimization is a local and global optimization process that can simulate wolf pack hunting. It can be roughly divided into four behavior modes: social hierarchy, tracking, encircling and attacking prey. It involves few parameters and is simple to implement. The mathematical derivation process of the GWPF algorithm is as follows.

Step 1: Set the state transition amount initial value.

The particles are extracted according to the important density function, and the high-dimensional particle set is selected by Sequential Importance Sampling (SIS). That is, N particles are collected at $t = 0$ to form a particle set $\{x_i^0, i = 1, \dots, N\}$. Define the recommended density function as shown in Eq. (10).

$$q(x_t) = p(x_t^i | x_{t-1}^i) \quad (10)$$

Then the particle set weight is shown in Eq. (11).

$$w(x_{t-1}^i) = w(x_{t-1}^i) p(y_t | x_{t-1}^i) = (1/\sqrt{2\pi\sigma}) \exp[-(y_t - y_t^i)^2 / \sigma] \quad (11)$$

Among them, y_t is the system observation. σ is the variance of Gaussian distribution, that is, $\sigma = 1$.

Step 2: The social hierarchy mechanism.

Take the particle set $\{x_i^0, i = 1, \dots, N\}$ at $t = 0$ as the initial population of the gray wolf algorithm. The weight $w(x_i^1:t)$ is used to characterize the individual fitness of gray wolves and carry out social hierarchical stratification. The gray wolf individual with the best adaptability in each generation population is selected to determine the position of the head wolf.

The layering mechanism is introduced into the PF algorithm. In the re-sampling stage, the particles are preferably selected, and the particles are rearranged to increase the diversity of particles and avoid particle degradation.

The α , β and δ wolves used to perceive prey determine the direction of the population to encircle and suppress prey. The candidate wolf pack ω is gradually updated following the position of the head wolf. When searching for prey, gray wolves gradually approach and surround. The mathematical expression is shown in Eq. (12).

$$\begin{cases} \mathbf{D} = \mathbf{C} \circ \mathbf{X}_p(t) - \mathbf{X}_i(t) \\ \mathbf{X}_i(t+1) = \mathbf{X}_i(t) - \mathbf{A} \circ \mathbf{D} \\ \mathbf{A} = 2a \mathbf{or}_1 - a, \mathbf{C} = 2\mathbf{r}_2 \end{cases} \quad (12)$$

Among them, \circ is the Hadamard product, which is a type of the matrix operation, also called the basic product. t represents the current iteration number. $\mathbf{X}_i(t)$ is the position vector of the current gray wolf. $\mathbf{X}_p(t)$ is the position vector of the current prey. \mathbf{r}_1 and \mathbf{r}_2 are random vectors on $[0, 1]$. $a \in [0, 2]$ is the convergence factor, and the whole process decreases from linear 2 to 0. \mathbf{A} and \mathbf{C} are the synergy coefficient vectors. \mathbf{D} is the distance vector from the prey to the gray wolf individual. \mathbf{A} a random value on $[-a, a]$. When a decreases linearly, the gray wolf moves between its current position and its prey. \mathbf{C} is a random value on $[0, 2]$, which represents random weights, which can effectively increase the diversity of particles and prevent the algorithm from falling into a local optimal solution.

Step 3: Update the fitness of the wolf.

Individual gray wolves have the potential to identify the location of their prey. In order to simulate the search behavior of gray wolves, the mathematical model for tracking prey is shown in Eq. (13).

$$\begin{cases} \mathbf{D}_\alpha = \mathbf{C}_1 \circ \mathbf{X}_\alpha(t) - \mathbf{X}_i(t), \mathbf{D}_\beta = \mathbf{C}_2 \circ \mathbf{X}_\beta(t) - \mathbf{X}_i(t) \\ \mathbf{D}_\delta = \mathbf{C}_3 \circ \mathbf{X}_\delta(t) - \mathbf{X}_i(t), \mathbf{X}_i^1(t) = \mathbf{X}_\alpha(t) - \mathbf{A}_1 \circ \mathbf{D} \\ \mathbf{X}_i^2(t) = \mathbf{X}_\beta(t) - \mathbf{A}_2 \circ \mathbf{D}, \mathbf{X}_i^3(t) = \mathbf{X}_\delta(t) - \mathbf{A}_3 \circ \mathbf{D} \end{cases} \quad (13)$$

Thus, the final position of the gray wolf individual is obtained, as shown in Eq. (14).

$$\mathbf{X}_i(t+1) = [\mathbf{X}_i^1(t) + \mathbf{X}_i^2(t) + \mathbf{X}_i^3(t)]/3 \quad (14)$$

Step 4: Determine the iterations number of the gray wolf algorithm.

If the gray wolf algorithm has not reached the set number of iterations, return to **step 2** and continue to select the head wolf position.

Step 5: Normalize particle weights.

The selected gray wolf population is used as the sampled particles in the PF algorithm, and the normalized weights of the particles are calculated, as shown in Eq. (15).

$$w(x_{1:t}^i) = w(x_{1:t-1}^i) / \sum_{i=1}^N w(x_{1:t}^i) \quad (15)$$

Finally, output the expected estimated value of the system state at the current discrete time.

Step 6: Calculate the number of the effective particles and determine whether to resample.

For particle degradation, the concept of relative efficiency (RNE) is proposed, as shown in Eq. (16).

$$(\text{RNE})^{-1} \approx \left[1 + \text{var}_{q(\bullet|y_{1:t})}(w) \right] \quad (16)$$

In the actual calculation process, the approximate value of the effective particle number based on RNE is shown in Eq. (17).

$$\begin{aligned} \hat{N}_{\text{eff}} &= N / \left[1 + \text{var}_{q(\bullet|y_{1:t})} \left[w(x_{1:t}^i) \right] \right] \\ &\approx 1 / \sum_{i=1}^N \left[w(x_{1:t}^i) \right]^2 \end{aligned} \quad (17)$$

If the number of effective particles sampled is less than the threshold set by estimation, re-sampling is performed. The posterior probability density is shown in Eq. (18).

$$p(x_{1:t} | y_{1:t}) \approx \sum_{i=1}^N w(x_{1:t}^i) \delta(x_{1:t} - x_{1:t}^i) \quad (18)$$

That is, the posterior probability density is resampled N times, so that $p(x_i^* | t) = x_j | t$, where $w_j k = 1/N$.

Step 7: Repeat (2) ~ (6) until the state estimation at all times is completed. The pseudo-code of the PF algorithm based on gray wolf optimization is shown in Tab. 4.

Tab. 4 PF algorithm based on gray wolf optimization

Algorithm 1. Pseudo-code of GWPF based SOC observation

Enter: initial particle set $\{x_i^0, i = 1, \dots, N\}$, observation y_t

Output: current moment particle set

1. **Procedure** SOC observation
2. **for** $k = 0$
3. Randomly generate initial the particle set
4. Initialize the gray wolf position and fitness of α, β, δ
5. **end for**
6. **while** not stop
7. **for** $t = 1, \dots, T$ do
8. **for** $i = 1, \dots, N$ do
9. Calculate particle weights using Eq. (11)
10. **end for**
11. **while** The iteration limit has not been reached
12. **for** $i = 1, \dots, N$ do
13. Update the gray wolf position using Eq. (12)
14. Calculate the final position using Eq. (13) and Eq. (14)
15. **end for**
16. **end while**
17. Normalized weights using Eq. (15)
18. Calculate the effective number of particles using Eq. (17)
19. **if** less than the number of effective particles
20. Particle resampling using Eq. (18)
21. **end if**
22. Update the particle set
23. **end for**
24. **end procedure**

To evaluate more intuitively the excellent performance of the optimization algorithm, the root mean square error (RMSE) and the mean absolute error (MAE) are respectively used for characterization, and the calculation formula is shown in Eq. (19).

$$\begin{cases} \text{RMSE} = \sqrt{\frac{1}{N} \sum_{i=1}^N (S_e - S_r)^2} \\ \text{MAE} = \frac{1}{N} \sum_{i=1}^N (S_e - S_r) \end{cases} \quad (19)$$

In Eq. (19), S_r is the actual value of SOC. S_e is the estimated value of SOC. N is the total number of training samples.

3. Experiments and results analysis

3.1. Test equipment and platform construction

The experiment is to study the working characteristics of

LIBs, using a ternary LIB as the main body of research, with a rated capacity of 70 Ah. The specific parameters are shown in Tab. 5.

Tab. 5 Performance parameters of ternary LIB

Battery parameters		Numerical value
Standard capacity (Ah)		70
Rated voltage (V)		3.65
Constant current and constant voltage charging (CC-CV)	Maximum charging current (C)	1
	Charge upper limit voltage (V)	4.2
Discharge at room temperature	Maximum continuous discharge current (C)	3
	End of discharge voltage (V)	2.75
Operating temperature	Recharge	0~45°C
	Discharge	-20~55°C

During the experiment, the battery test system (NEWARE BTS-4000) and thermostat (SETH-Z-040L) were used to charge and discharge LIBs. It can effectively avoid the model parameters change due to temperature changes under the same working condition test. The experimental test platform is shown in Fig. 2.

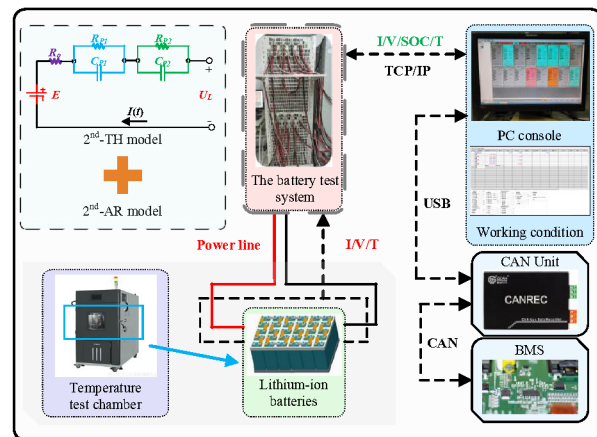


Fig. 2. Experimental test platform

Based on the above experimental test platform, the RLS method with a forgetting factor of 0.985 is used for online parameter identification and in-depth study of the LIBs internal reaction mechanism.

3.2. Identification results and model validation

The hybrid pulse power characteristic (HPPC) test experiment was carried out on the ternary LIB selected in

the experiment. Under the environmental condition of 23 °C, the operating LIB characteristics were studied by pulse charging and discharging. The experiment flow chart is shown as in Fig. 3.

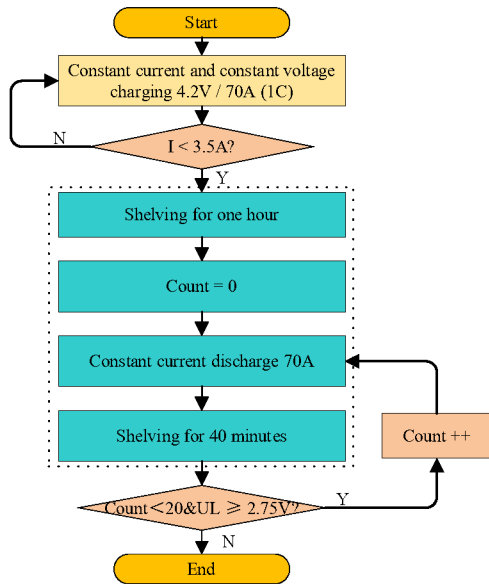
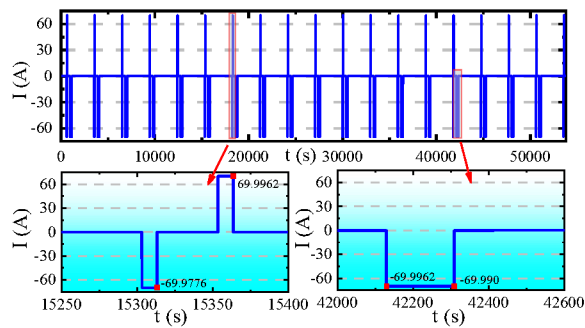


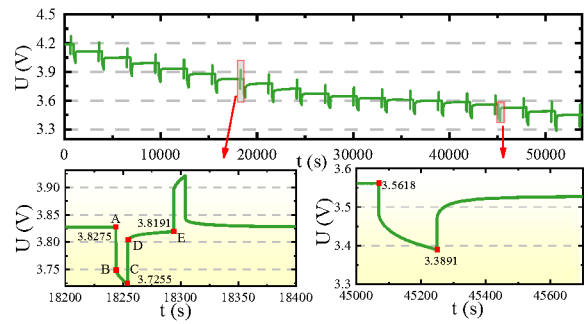
Fig. 3. Experiment flow chart

Under the premise of considering the safe operation of LIBs, the HPPC experiment was used to carry out cyclic pulse charging and discharging. Every time a pulse charge and discharge is completed, the battery is discharged with a constant current of 5% capacity, and the experiment is stopped until the battery is exhausted.

Collect the data to get the battery current and voltage change curve. And get the single pulse charge and discharge curves, as shown in Fig. 4.



(a) Current diagram



(b) Voltage diagram

Fig. 4. HPPC working condition current and voltage curve

During the cycle operation, the last moment of the battery in the rest state is recorded as the OCV at this time. The data is recorded, visualized, and fitted to realize the OCV-SOC discrete points to a function. Taking into account the subsequent code running rate and the load impact of the processor, a 5-order polynomial is selected, and the functional relationship is shown in Eq. (20).

$$U_{oc} = 3.783 * SOC^5 - 13.7 * SOC^4 + 18.44 * SOC^3 - 10.58 * SOC^2 + 3.0001 * SOC + 3.232 \quad (20)$$

The entire fitting process is data collected when the LIB was in a static state for predicting the actual amount of power remaining in the battery.

Among them, Fig. 4 (b) can be seen from the end-to-end voltage results, AB and CD are the discharge start and discharge end stages, respectively. The terminal voltage changes drastically mainly caused by the ohmic internal resistance of the LIB. Because the high-fidelity second-order autoregressive model contains the RC network, when the circuit structure or parameter changes suddenly and when the external excitation is zero, the system energy is only excited by the initial energy storage of the capacitor in the RC network, provides electrical energy, and a zero-input response occurs. The voltage at both ends of the capacitor cannot jump, so the voltage at the LIB terminal rises gently after point D.

Considering the reasons for the curve change in the whole process, and verifying the superiority of the second-order autoregressive model, model verification is required. The model identification results obtained by using the forgetting factor least square method are shown in Tab. 6.

Tab. 6 Parameter identification results

Parameter	g0	g1	g2
R_o	0.001496	-0.002944	0.01056
R_1	0.0001814	-0.001431	0.005318

C_1	1.951E4	-3.362E5	2.568E6
R_2	0.0007689	9.004E-5	-0.01079
C_2	1.225E4	-2.201E4	9.978E5
Parameter	g3	g4	g5
R_o	-0.01961	0.01793	-0.006334
R_1	-0.009766	0.008982	-0.003249
C_1	-6.382E6	6.467E6	-2.314E6
R_2	0.03069	-0.02698	0.006685
C_2	-3.33E6	3.92E6	-1.549E6

According to Tab. 6, it is a characterization of the relationship between circuit parameters and SOC fitting. The identification parameters obtained from the Tab. 6 are verified in MATLAB. Verify the accuracy of the improved model, and get the terminal voltage output and error tracking curve, as shown in Fig. 5.

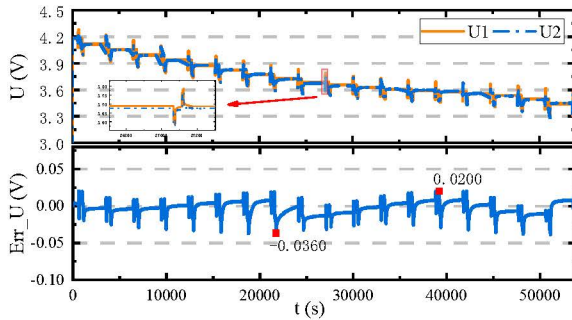


Fig. 5. LIB equivalent model verification

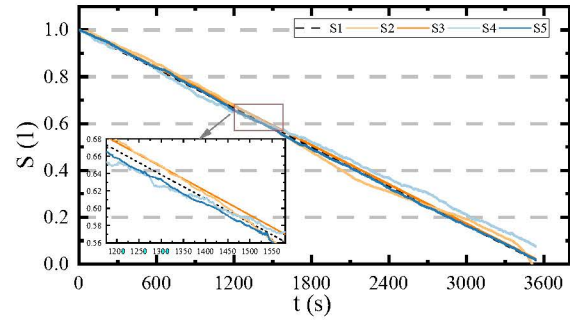
Among them, U1 represents the simulated voltage, and U2 represents the actual voltage. It can be seen directly from the Fig. 5 that the maximum error deviation of the output voltage is 0.0360V, and the accuracy is over 99%, which is well adapted to the performance of the internal reaction mechanism of the LIB. Due to the drastic change of the terminal voltage during the HPPC process, the error tracking curve fluctuates. But the entire error changes within a certain range, and there is no jump at a certain moment. Therefore, the response effect of LIBs can be well replaced, and it is reasonable.

3.3. Experimental results under constant current cycle

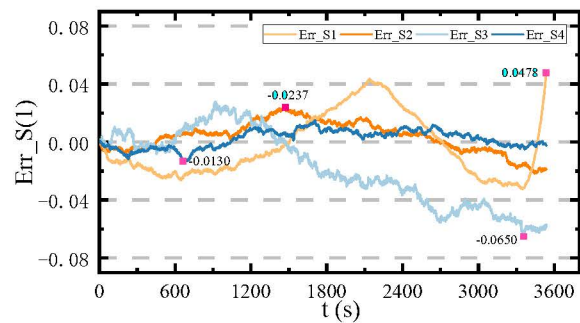
To verify the performance of the SOC estimation based on the GWPF algorithm and to analyze the generalization, robustness, and superiority of the improved algorithm, a multi-condition experimental test was carried out and compared with the traditional SOC estimation methods.

Experiments were conducted under complex working conditions, and 100 sets of sample data are used for testing.

First of all, under constant current conditions, discharge at a rate of 1C. By comparing with the traditional SOC estimation methods, the estimated curve and error curve are obtained, as shown in Fig. 6.



(a) SOC estimation curve



(b) Error tracking curve

Fig. 6. Results under constant current condition

Among them, S1, S2, S3, S4, S5 represent the true value, EKF estimated value, UKF estimated value, PF estimated value and GWPF estimated value respectively. Err_S1, Err_S2, Err_S3, Err_S4 are EKF estimation error, UKF estimation error, PF estimation error and GWPF estimation error, respectively. As shown in Fig. 6 (a), the SOC estimation is a curve with a continuously changing slope. It is caused by the non-linearity and instability characteristics of the experimental data measured by the LIB. Analysis of the experimental data reveals the performance expression of EKF, UKF, PF, GWPF algorithm is shown in Tab. 7.

Tab. 7 Comparison of estimated performance of various algorithm under constant current condition

Method	EKF	UKF	PF	GWPF
Error/%	4.78	2.37	6.50	1.30
RMSE/%	4.31	1.82	3.76	0.92
MAE/%	2.83	1.39	3.10	0.88
Running time/s	3.077	6.914	5.166	9.891

According to the data analysis in Tab. 7, compared with traditional EKF, UKF, PF, the maximum estimation error of

the GWPF algorithm for estimating the LIB SOC is 1.30%. The maximum errors of RMSE and MAE are 0.92% and 0.88%, respectively. The running time is 9.891s. Therefore, the improved PF estimation method has higher accuracy and convergence.

3.4. Experimental results under the DST cycle

To further, verify the portability of the algorithm, the experimental analysis is carried out under the dynamic stress test (DST) conditions, and the DST operating conditions data are obtained, as shown in Fig. 7.

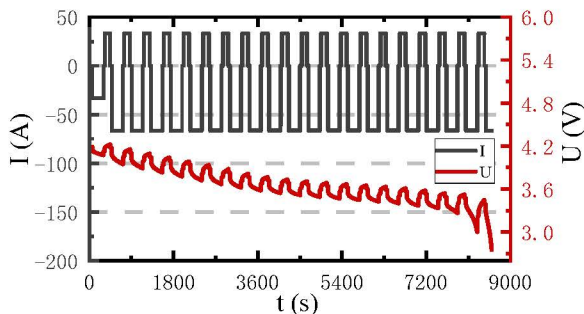


Fig. 7. DST working condition data

Based on the above working conditions, the experimental data is embedded in the SOC estimation method, and the SOC estimation and error tracking curves obtained under DST working conditions are as shown in Fig. 8.

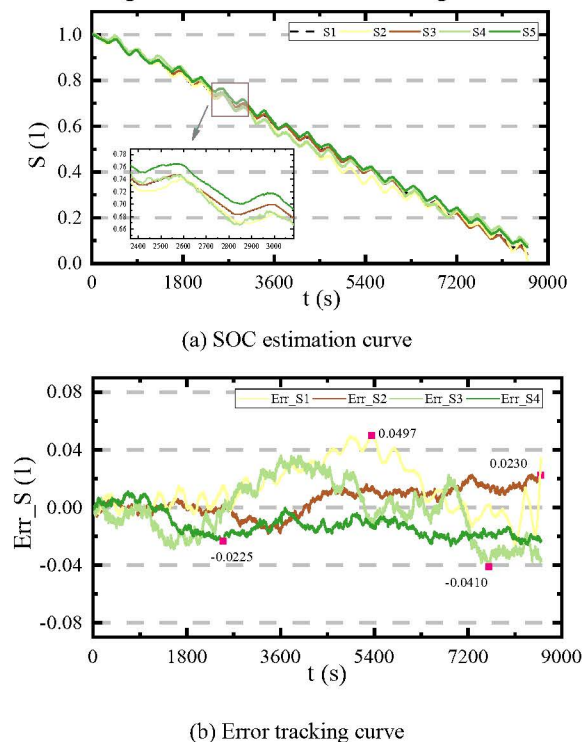


Fig. 8. Results under DST

The traditional estimation methods and the improved algorithm are compared and analyzed, and the estimation performance comparison of each algorithm is shown in Tab. 8.

Tab. 8 Comparison of estimated performance of various algorithm under DST condition

Method	EKF	UKF	PF	GWPF
Error/%	4.97	2.30	4.10	2.25
RMSE/%	2.89	1.68	2.13	1.35
MAE/%	2.47	1.29	1.83	1.07
Running time/s	6.723	15.317	16.164	22.912

According to the data analysis in Tab. 8, compared with other algorithms, the maximum estimation error of the GWPF algorithm for estimating the LIB SOC is 2.25%. The maximum errors of RMSE and MAE are 1.35% and 1.07%, respectively. The running time is 22.912s.

Regardless of the constant current condition or the DST condition, it can be seen that the proposed novel GWPF algorithm has a high-precision SOC estimation effect, strong transplantability, high stability and fast convergence. It proves that the improved algorithm proposed in this paper has high practical value and provides a solid theoretical basis for subsequent practical applications.

4. Conclusions

To seek an accurate model construction and efficient state monitoring with collaborative estimation, this paper proposes a novel GWPF algorithm for LIBs SOC estimation. This algorithm can effectively compensate for the particle depletion and weight degradation in the traditional PF algorithm. To verify the GWPF algorithm effectiveness, a high-fidelity second-order autoregressive model was constructed to characterize the dynamic characteristics of LIBs. The forgetting factor recursive least square (FFRLS) method was used to identify model parameters, and to evaluate the SOC estimation performance under complex working conditions. Experimental results show that based on the model verification of HPPC operating conditions, the maximum error deviation between the voltage simulation value and the actual value is 0.0360 V, which accounts for 0.857% of the battery's nominal voltage with strong fidelity and good traceability. On this basis, experimental verification was carried out under constant current discharge and DST conditions. The GWPF algorithm has strong generalization in estimating the LIBs SOC, and the error is basically stable within 2%, the running time is short,

the execution efficiency is high, and achieving high-precision estimation, which confirms that the GWPF algorithm has an excellent performance in predicting the remaining power of LIBs. Through actual operation analysis and verification, the algorithm can increase the diversity of particles, realize accurate estimation of the state of LIBs, and provide useful explorations for the quality evaluation, reliability evaluation, and popularization and application of ternary LIBs.

Acknowledgments

The work was supported by National Natural Science Foundation of China (No. 61801407), China Scholarship Council (No. 201908515099) and Fund of Robot Technology Used for Special Environment Key Laboratory of Sichuan Province (No. 18kftk03).

References

1. Yang, J.F., et al., *Online state-of-health estimation for lithium-ion batteries using constant-voltage charging current analysis*. Applied Energy, 2018. **212**: p. 1589-1600.
2. Chen, X.B., X.P. Chen, and X.W. Chen, *A novel framework for lithium-ion battery state of charge estimation based on Kalman filter Gaussian process regression*. International Journal Of Energy Research, 2021.
3. Wei, Z.B., et al., *Future smart battery and management: Advanced sensing from external to embedded multi-dimensional measurement*. Journal Of Power Sources, 2021. **489**.
4. Guo, Y.J., et al., *A compact and optimized neural network approach for battery state-of-charge estimation of energy storage system*. Energy, 2021. **219**.
5. Schmid, M., et al., *Active Model-Based Fault Diagnosis in Reconfigurable Battery Systems*. Ieee Transactions on Power Electronics, 2021. **36**(3): p. 2584-2597.
6. Jiang, C., et al., *A state-of-charge estimation method of the power lithium-ion battery in complex conditions based on adaptive square root extended Kalman filter*. Energy, 2021. **219**.
7. Yan, Q.C., et al., *State of Charge Estimation for Lithium-Ion Battery via MILS Algorithm Based on Ensemble Kalman Filter*. International Journal Of Photoenergy, 2021. **2021**.
8. Shen, D.X., et al., *A novel online method for predicting the remaining useful life of lithium-ion batteries considering random variable discharge current*. Energy, 2021. **218**.
9. Liu, Z., et al., *A State of Charge Estimation Method for Lithium-Ion Battery Using PID Compensator-Based Adaptive Extended Kalman Filter*. Complexity, 2021. **2021**.
10. Wei, Z.B., et al., *Noise-Immune Model Identification and State-of-Charge Estimation for Lithium-Ion Battery Using Bilinear Parameterization*. Ieee Transactions on Industrial Electronics, 2021. **68**(1): p. 312-323.
11. Wei, X., Y.M. Mo, and Z. Feng, *Lithium-ion Battery Modeling and State of Charge Estimation*. Integrated Ferroelectrics, 2019. **200**(1): p. 59-72.
12. Qu, S.F., et al., *A Fast Online State of Health Estimation Method for Lithium-Ion Batteries Based on Incremental Capacity Analysis*. Energies, 2019. **12**(17).
13. Chang, C.C., Y.P. Zheng, and Y. Yu, *Estimation for Battery State of Charge Based on Temperature Effect and Fractional Extended Kalman Filter*. Energies, 2020. **13**(22).
14. Xiong, R., et al., *An electrochemical model based degradation state identification method of Lithium-ion battery for all-climate electric vehicles application*. Applied Energy, 2018. **219**: p. 264-275.
15. Zhang, L.J., et al., *Comparative Research on RC Equivalent Circuit Models for Lithium-Ion Batteries of Electric Vehicles*. Applied Sciences-Basel, 2017. **7**(10).
16. He, Y., et al., *Equivalent hysteresis model based SOC estimation with variable parameters considering temperature*. Journal Of Power Electronics, 2021. **21**(3): p. 590-602.
17. Wu, X.G., X.F. Li, and J.Y. Du, *State of Charge Estimation of Lithium-Ion Batteries Over Wide Temperature Range Using Unscented Kalman Filter*. Ieee Access, 2018. **6**: p. 41993-42003.
18. Wang, S.L., et al., *The parameter identification method study of the splice equivalent circuit model for the aerial lithium-ion battery pack*. Measurement & Control, 2018. **51**(5-6): p. 125-

- 137.
19. Meng, J.H., et al., *A Novel Multiple Correction Approach for Fast Open Circuit Voltage Prediction of Lithium-Ion Battery*. Ieee Transactions on Energy Conversion, 2019. **34**(2): p. 1115-1123.
20. Campestrini, C., S. Kosch, and A. Jossen, *Influence of change in open circuit voltage on the state of charge estimation with an extended Kalman filter*. Journal Of Energy Storage, 2017. **12**: p. 149-156.
21. Bao, Y., W.B. Dong, and D.A. Wang, *Online Internal Resistance Measurement Application in Lithium Ion Battery Capacity and State of Charge Estimation*. Energies, 2018. **11**(5).
22. Li, X.Y., et al., *Multi-state joint estimation for a lithium-ion hybrid capacitor over a wide temperature range*. Journal Of Power Sources, 2020. **479**.
23. Xiong, X., et al., *A novel practical state of charge estimation method: an adaptive improved ampere-hour method based on composite correction factor*. International Journal Of Energy Research, 2020. **44**(14): p. 11385-11404.
24. Garcia, R.V., et al., *Nonlinear filtering for sequential spacecraft attitude estimation with real data: Cubature Kalman Filter, Unscented Kalman Filter and Extended Kalman Filter*. Advances In Space Research, 2019. **63**(2): p. 1038-1050.
25. Liu, H., et al., *Comparisons on Kalman-Filter-Based Dynamic State Estimation Algorithms of Power Systems*. Ieee Access, 2020. **8**: p. 51035-51043.
26. Xu, W.H., et al., *Novel reduced-order modeling method combined with three-particle nonlinear transform unscented Kalman filtering for the battery state-of-charge estimation*. Journal Of Power Electronics, 2020. **20**(6): p. 1541-1549.
27. Wang, K., et al., *State of Charge (SOC) Estimation of Lithium-ion Battery Based on Adaptive Square Root Unscented Kalman Filter*. International Journal Of Electrochemical Science, 2020. **15**(9): p. 9499-9516.
28. Shi, H.T., et al., *A Novel Dual Correction Extended Kalman Filtering Algorithm for The State of Charge Real-Time Estimation of Packing Lithium-Ion Batteries*. International Journal Of Electrochemical Science, 2020. **15**(12): p. 12706-12723.
29. Xia, B.Z., et al., *Online Parameter Identification and Joint Estimation of the State of Charge and the State of Health of Lithium-Ion Batteries Considering the Degree of Polarization*. Energies, 2019. **12**(15).
30. Yang, K., Y.G. Tang, and Z. Zhang, *Parameter Identification and State-of-Charge Estimation for Lithium-Ion Batteries Using Separated Time Scales and Extended Kalman Filter*. Energies, 2021. **14**(4).
31. Ben Sassi, H., F. Errahimi, and N. ES-Sbai, *State of charge estimation by multi-innovation unscented Kalman filter for vehicular applications*. Journal Of Energy Storage, 2020. **32**.
32. Zhu, R., et al., *Co-estimation of model parameters and state-of-charge for lithium-ion batteries with recursive restricted total least squares and unscented Kalman filter*. Applied Energy, 2020. **277**.
33. Zhang, S.Z., X. Guo, and X.W. Zhang, *An improved adaptive unscented kalman filtering for state of charge online estimation of lithium-ion battery*. Journal Of Energy Storage, 2020. **32**.
34. Liu, X.T., et al., *A Dynamic State-of-Charge Estimation Method for Electric Vehicle Lithium-Ion Batteries*. Energies, 2020. **13**(1).
35. Qiu, X.H., W.X. Wu, and S.F. Wang, *Remaining useful life prediction of lithium-ion battery based on improved cuckoo search particle filter and a novel state of charge estimation method*. Journal Of Power Sources, 2020. **450**.
36. Yang, X.L., et al., *Battery states online estimation based on exponential decay particle swarm optimization and proportional-integral observer with a hybrid battery model*. Energy, 2020. **191**.
37. Wang, S.L., et al., *A novel safety assurance method based on the compound equivalent modeling and iterate reduce particle-adaptive Kalman filtering for the unmanned aerial vehicle lithium ion batteries*. Energy Science & Engineering, 2020. **8**(5): p. 1484-1500.

- 1
2
3
4
5
6
7
8
9
10
11
12
13
14
15
16
17
18
19
20
21
22
23
24
25
26
27
28
29
30
31
32
33
34
35
36
37
38
39
40
41
42
43
44
45
46
47
48
49
50
51
52
53
54
55
56
57
58
59
60
38. Wei, W.H., et al., *Adaptive Square-Root Unscented Particle Filtering Algorithm for Dynamic Navigation*. Sensors, 2018. **18**(7).
39. Wang, Y.J. and Z.H. Chen, *A framework for state-of-charge and remaining discharge time prediction using unscented particle filter*. Applied Energy, 2020. **260**.
40. Javid, G., D.O. Abdeslam, and M. Basset, *Adaptive Online State of Charge Estimation of EVs Lithium-Ion Batteries with Deep Recurrent Neural Networks*. Energies, 2021. **14**(3).
41. Ragone, M., et al., *Data driven estimation of electric vehicle battery state-of-charge informed by automotive simulations and multi-physics modeling*. Journal Of Power Sources, 2021. **483**.
42. Khan, N., et al., *Batteries State of Health Estimation via Efficient Neural Networks With Multiple Channel Charging Profiles*. Ieee Access, 2021. **9**: p. 7797-7813.
43. Yao, L., et al., *An Intelligent Fault Diagnosis Method for Lithium Battery Systems Based on Grid Search Support Vector Machine*. Energy, 2021. **214**.
44. Zhou, Z.K., et al., *An efficient screening method for retired lithium -ion batteries based on support vector machine*. Journal Of Cleaner Production, 2020. **267**.